ENVIRONMENTAL RESEARCH
LETTERS

PURPOSE-LED PUBLISHING™ Part of the ENVIRONMENTAL RESEARCH SERIES

LETTER • OPEN ACCESS

Climate shapes baseflows, influencing drought severity

To cite this article: Masoud Zaerpour *et al* 2025 *Environ. Res. Lett.* **20** 014035

ENVIRONMENTAL RESEARCH
LETTERS

LETTER

Climate shapes baseflows, influencing drought severity

Masoud Zaerpour[1,*], **Shadi Hatami**[1], **André S Ballarin**[1,2], **Simon Michael Papalexiou**[1,3], **Alain Pietroniro**[1] and **Jan Franklin Adamowski**[4,5]

[1] Department of Civil Engineering, Schulich School of Engineering, University of Calgary, Calgary, Canada
[2] Department of Hydraulics and Sanitation, São Carlos School of Engineering, University of São Paulo, São Paulo, Brazil
[3] Faculty of Environmental Sciences, Czech University of Life Sciences, Prague, Czech Republic
[4] Department of Bioresource Engineering, McGill University, Montreal, Canada
[5] United Nations University Institute for Water,Environment, and Health (UNU-INWEH), Montreal, Canada
[*] Author to whom any correspondence should be addressed.

E-mail: masoud.zaerpour@ucalgary.ca

Keywords: drought, baseflow, streamflow, climate

OPEN ACCESS

RECEIVED
19 June 2024

REVISED
31 October 2024

ACCEPTED FOR PUBLICATION
26 November 2024

PUBLISHED
17 December 2024

Abstract

Baseflow, the sustained flow from groundwater, lakes, and snowmelt, is essential for maintaining surface water flow, particularly during droughts. Amid rising global water demands and climate change impacts, understanding baseflow dynamics is crucial for water resource management. This study offers new insights by assessing baseflow controls at finer temporal scales and examining their relationship with hydrological drought flows. We investigate how climatic factors influence seasonal baseflow in 7138 global catchments across five major climate regions. Our analysis identifies precipitation as the primary driver, affecting 58.3% of catchments, though its impact varies significantly across different climates. In temperate regions, precipitation dominates (61.9% of catchments), while in tropical regions, evaporative demand is the leading factor (47.3%). Snow fraction is particularly crucial in both snow-dominated (20.8%) and polar regions (48.5%). Negative baseflow trends generally emerge where the effects of evaporative demand or snow fraction outweigh those of precipitation. Specifically, in northern regions and the Rocky Mountains, where snow fraction predominantly controls baseflow changes, a negative trend is evident. Similarly, in tropical catchments, where evaporative demand drives baseflow changes, this also leads to a negative trend. Additionally, our findings indicate that baseflow changes are closely linked to hydrologic drought severity, with concurrent trends observed in 69% of catchments. These findings highlight the relationship between baseflow changes, the severity of hydrologic drought and shifts in precipitation, evaporative demand, and snow dynamics. This study provides crucial insights for sustainable water resource planning and climate change adaptation, emphasizing the importance of managing groundwater-fed river flows to mitigate drought impacts.

1. Introduction

Baseflow, the perennial flow component of streamflow generated by groundwater storage, wetlands, lakes, melting snow and glaciers [1–3], is crucial in sustaining surface water flow and supporting river ecosystems. As a relatively stable streamflow component, baseflow becomes indispensable during drought, acting as a vital supply for effective water resource planning and management [4, 5]. During meteorological drought conditions, baseflow serves as a buffer against hydroclimatic variations and influences the propagation and severity of water deficits, ultimately impacting society's vulnerability to these extreme events [6–8]. Therefore, understanding baseflow dynamics, controlling mechanisms, and their role in hydrologic drought severity is essential for mitigating drought impacts on water availability and ecosystem health [9–17].

Many studies have explored changes in baseflow, revealing diverse patterns across different parts of the globe. For instance, in the US Midwest, a significant increase in baseflow from May to September was identified for a series of basins [18], while in the Missouri River Basin, an overall rise in the number of stations with positive baseflow slopes from 1950 to

2014 was observed [10]. China's Yellow River Basin saw a general decline in annual baseflow from 1950–2000 [19]. Southern Africa exhibited increases and then decreases in baseflow from 1981–2018, while northern Africa experienced consistently decreasing trends from 1950–2018 [20]. Studies in Australia, such as those focused on the Murray–Darling Basin, have highlighted the potential consequences of climate change, including predicting reductions in river baseflow and adverse impacts on groundwater-dependent ecosystems [21–25]. In Central Europe, studies have highlighted the impacts of climate and catchment controls on baseflow changes, revealing a highly variable pattern of trends for baseflow across the region, with low flows exhibiting more frequent downward trends [4, 26]. Other studies have focused on regional analysis of groundwater, incorporating observation wells. However, while well time series are often abundant in space, they are challenging to extrapolate from point to catchment scale and may not reflect catchment-scale groundwater storage [27–29].

Despite growing concerns over how human activity and global climate change may affect water resources, the impact of climate change on baseflow changes and its relationship to hydrological drought is still relatively understudied [1, 5, 30]. One of the primary drivers of baseflow changes is climate, with precipitation, potential evapotranspiration (ET_p), and snow fraction being among the most significant variables [30–37]. When precipitation increases, more water can permeate the ground and contribute to groundwater recharge, which usually leads to an increase in baseflow [30, 37]. Hence, climate-change-driven changes in the form of precipitation (*e.g.* a shift from snow to rain), can also affect baseflow [1]. For instance, a decrease in snow cover, driven by reduced albedo and increased sublimation, can decrease seasonal streamflow components [38, 39]. Similarly, baseflow may decline if fewer glaciers are present and lesser snow melt occurs in summer [1]. Baseflow changes have also been related to increases in ET_p in some places due to rising temperatures [40]. As more water is lost to the atmosphere and less water is available for groundwater recharge, a higher ET_p can decrease baseflow [40]. For instance, studies conducted in the Upper Colorado River basin have indicated that greater climate-change-driven increases in evapotranspiration relative to precipitation may reduce baseflow [30]. In contrast, a Canadian study found that warmer temperatures and greater snow cover resulted in greater baseflow [41].

Many studies examining streamflow components have employed coarse temporal perspectives to assess dominant climate and physiographic controls of catchment water partitioning [37, 42–47]. Overall, some of these studies rely on Budyko-based frameworks, initially developed for spatial, between-catchment analyses under long-term temporal scales. Nevertheless, given space-time asymmetry, their use for analyzing water availability sensitivity and dynamics at finer temporal scales is debatable [48]. In fact, the Budyko framework, though informative [37, 43, 44, 49, 50], disregards a substantial amount of hydrological information and the interaction of multiple factors that could affect baseflow dynamics at finer temporal scales. Furthermore, the Budyko framework is not fully developed for baseflow partitioning, and geographical differences in baseflows between catchments may arise due to various factors such topography, soil properties [51–54], and vegetation [55, 56].

To address this challenge and gain insight into the intricate interplay of climate variables and baseflow at finer time scales, we employ the Peter-Clark Momentary Conditional Independence Plus (PCMCI+) algorithm [57–59]—recently applied in Earth System sciences—to systematically explore causal relationships among hydroclimatic variables. PCMCI+ offers a framework for identifying directional dependencies among variables by leveraging time series data, making it particularly suited for analyzing the complex interplay between climatic factors and baseflow. Recent studies in hydrometeorology have demonstrated the effectiveness of PCMCI+ in capturing both direct and indirect causal pathways in baseflow and streamflow analysis, providing new insights into how drivers interact to impact water resources [57, 60–64]. We investigate the implications of baseflow changes for hydrological droughts, marking this as a first evaluation of the significance of baseflow alterations in the context of hydrological drought dynamics. Depletion of the groundwater-sustained component of river flow (*i.e.* baseflow) during persistent droughts can pose additional pressure on water security [4, 65–67]. This necessitates the identification of regions susceptible to co-occurrence of baseflow loss and hydrological drought conditions. The structure of the paper is as follows. First, we examine the climatic factors influencing baseflow changes; subsequently, we explore how baseflow loss is related to hydrological drought; finally, we identify catchments where baseflow loss and hydrological drought occur simultaneously.

2. Data and methods

2.1. Data

Data of the studied watersheds was extracted from the Caravan global dataset [68], which standardizes and aggregates large-sample hydrology datasets, including the CAMELS datasets [69–73]. Caravan is a comprehensive hydrological dataset that includes

catchment attributes and streamflow data for various locations. The Caravan dataset was selected to ensure a globally consistent and spatially coherent dataset, as it integrates CAMELS hydrological data with ERA5-Land meteorological forcings, facilitating global comparative studies across diverse geographical settings. We selected 7138 catchments with at least 15 years of data from 1981–2020. The catchments exhibit diverse sizes, ranging from 10 to 2600 km^2. The Caravan dataset can be extracted from https://zenodo.org/records/7387919.

We used daily streamflow, temperature, precipitation, and ET_p data. The two climate controls of baseflow, including seasonal precipitation and ET_p, were directly calculated from the daily meteorological data. In Caravan, ET_p is derived using the Penman–Monteith equation, integrating climatic factors such as temperature, humidity, wind speed, and radiation [74–76]. A simple temperature-based threshold served to calculate snow fraction (*i.e.* the portion of precipitation that falls as snow). If the average temperature for a given day remained below 1 °C, all precipitation was classified as snowfall [77, 78]. Conversely, when temperatures exceeded 1 °C, the precipitation was categorized as rainfall. It is important to note that total precipitation includes both rain and snow. An alternative threshold of 0 °C [79] was also explored, with consistent results, regardless of the chosen method for estimating snowfall.

2.2. Baseflow and hydrological drought estimations

Baseflow was estimated using a one-parameter recursive filter developed by Lyne and Hollick [49, 80–84], commonly used in the literature [41, 50, 85–87] to decompose streamflow into its constituent components, namely baseflow and direct flow:

$$q_t = Q_t - \left(\beta q_{t-1} + \frac{1+\beta}{2}.(Q_t - Q_{t-1})\right) \quad (1)$$

where q_t is the filtered quick response on day t, Q_t is the original streamflow, and β is the filter parameter (set at 0.925; a commonly-used value in hydrological studies [44, 50, 85, 87–89]). We applied the recursive filter iteratively three times (forward-back-forward) to filter off flood peaks from the original streamflow time series. This separates the slow, groundwater-derived baseflow from the rapid, rainfall-induced direct flow. Seasonal baseflow values are then calculated from the daily values for the analysis, with the seasons defined as follows: spring (March to May), summer (June to August), fall (September to November), and winter (December to February).

However, different streamflow partitioning methods, including the graphical method developed by the UK Institute of Hydrology [90], Fixed interval graphical method from the HYSEP program [91], Eckhardt filter [3], and Chapman filter [92] have been previously applied. To address the inherent uncertainty in streamflow partitioning [49], we conducted an additional analysis comparing the three-pass Lyne-Hollick filter with other streamflow partitioning methods (figure S1 in the appendix). The high correlation values, ranging from 0.90 to 1.0, indicate a strong consistency between the methods, particularly between the LH method and the others. Therefore, we opted to keep using the three-time running LH filter.

Hydrological drought is generally defined by a deficiency in the volume of surface water supply [93, 94]. It is often characterized by low streamflow conditions. Here, we use the widely used 7 d low flow, which is the annual series of the minimum values of mean discharge over any seven consecutive days [95]. This results in one annual minimum value for each year.

2.3. Causal discovery algorithm

Here, we used the PCMCI+ causal discovery algorithm [58, 59, 61]—recently developed and applied in Earth system sciences—to examine the role of climate on temporal changes of baseflow at the seasonal time scale. Non-climatic factors also affect baseflow changes, including topography, soil properties [51–54], and vegetation [55, 56]. We focus only on the climate control of baseflow changes as it can explain most of the variability in baseflows. In particular, we explore the causal effect of precipitation, snow fraction, and evaporative demand on baseflow changes using empirical data [43, 96–98]. The PCMCI+ algorithm can outperform correlation analysis, identifying linkages that traditional correlation analysis miss [64]. Moreover, it excels at accounting for common drivers and detecting indirect links, distinguishing itself from other causal discovery methods, such as Granger causality [57, 58, 99].

The initial step involved constructing a directed acyclic graph to unveil causal relationships between variables. This graphical representation outlines the system's causal structure, with nodes representing variables and directed edges signifying causal relationships. This algorithm begins with a fully connected graph and then iteratively evaluates the removal of links between variables, considering expanding cardinality conditioning sets. The algorithm has two stages. First, the PC_1, a Markov set discovery algorithm based on the PC-stable algorithm [100], eliminates spurious links through iterative independence testing. Here, we use linear partial correlation for the conditional independence test. The significance level of the independence test is set to 0.05, allowing the PC algorithm to converge to only a few relevant conditions. In the second step, the momentary conditional independence (MCI) test uses the estimated conditions found in step one to infer a causal link. While the primary goal of the PCMCI+ algorithm

is to detect the causal graph, the MCI test statistics also provide a well-interpretable measure of a normalized causal strength (MCI test statistics value), used to determine the strength of causal links between variables [60, 101]. The absolute MCI test statistic value [57, 58, 99, 102] ranges from 0 (weakest) to 1 (strongest). The Python software for estimating the causal network can be obtained from https://tocsy.pik-potsdam.de/tigramite.php.

3. Results

3.1. Climatic controls on baseflow changes: regional patterns and global assessment

First, we perform a global assessment of the causal strength of specific climate controls on baseflow changes (figure 1), thus providing insights into the varying impacts of climate controls on baseflow across distinct climate zones. The causal link strength (MCI values) for the three climate controls are shown in figures 1(a)–(c). Figures 1(d)–(h) display histograms illustrating the distribution of absolute causal strengths across the five major climate zones.

Globally, precipitation stands out as the dominant factor influencing baseflow, with a noteworthy expected MCI of 0.45. Evaporative demand follows with a substantial yet lesser impact (MCI = 0.30), while snow fraction contributes with an expected MCI of 0.25. In the tropical zone, precipitation and evaporative demand play significant roles, with expected MCI values of 0.42 and 0.41, respectively. In arid climates, precipitation is identified as the dominant factor (MCI = 0.40), while in temperate climates, a similar pattern emerges. Conversely, in cold climates, snow fraction becomes more influential than evaporative demand (MCI = 0.26), and precipitation retains significance (MCI = 0.39). In polar climates, snow fraction prevails (MCI = 0.40), and precipitation maintains significant causal strength (MCI = 0.33).

To assess the impact of dataset choice on our results, we conducted an additional analysis using four CAMELS datasets that utilize gauge station data for climate forcings. As shown in figure S2 in the appendix, the overall patterns of climate controls on baseflow remained consistent across datasets. Variations were observed in only 4.2% of catchments for precipitation, primarily in northern Brazil and the eastern US, and in 7% of catchments for evaporative demand. It is worth noting that while there may be differences in the absolute values between datasets, our focus here is on the causal effect of climate controls on baseflow, which largely remains consistent.

The analysis of causal strength in figure 1 and the dominant control in figure S3 reveal that while precipitation holds some significance as a control of baseflow changes in 73% of catchments, it is the primary control in only 58.3% of catchments globally. This underscores the critical role of precipitation variability in modulating baseflow both temporally and spatially. To determine the primary control, we ranked the three factors—precipitation, evaporative demand, and snow fraction—based on their MCI values at each gauge station. Evaporative demand emerges as the second most significant factor, in 17% of catchments, indicating that it can substantially alter baseflow, particularly under warming conditions. The evaporative demand holds its significance in the control of baseflow in 42.3% of studied catchments. Snow fraction is the primary factor affecting baseflow in 12% of catchments, and exhibiting a significant control in 24.7% of studied catchments. This highlights the importance of the shift from snowmelt and snow accumulation processes in cold regions toward greater rain due to climate warming. The remaining catchments are governed by other factors not included in our analysis such as topography, soil properties, and vegetation, suggesting a complex interplay of additional controls.

The preceding analysis showed the dominance of precipitation in governing baseflow changes. To better understand the impact of climatic drivers on baseflow changes at the regional scale, we examine the prevalence of the three key climatic factors across five major Köppen climate regions (figure 2). Each bar represents a climatic region, and colors denote climatic factors. The colored segments indicate the percentage of catchments where a particular climatic driver predominantly controls baseflow. Precipitation emerges as the primary driver in four out of five climate regions, reaching its highest relative occurrence at 61.89% in the temperate climate zone and its lowest at 21.21% in the polar climate zone. Evaporative demand is the second most influential factor, with its peak occurrence (47.31%) in the tropical climate zone and the lowest (9.02%) in the snow climate zone. Snow fraction significantly impacts baseflow across four out of five climate zones, with the highest occurrence (48.48%) in the polar climate zone and the lowest (6.53%) in the temperate climate zone. Beyond climatic factors, it is important to acknowledge the contribution of other variables in explaining baseflow changes, with the polar climate region exhibiting the highest contribution (21.21%).

3.2. Understanding the relationship between baseflow changes and hydrological drought

The previous analysis unveils the impact of climate controls on baseflow, yet lacks insights into the intensity of baseflow changes across catchments. To assess the severity of baseflow alterations, we calculate the linear regression trend of the normalized annual baseflows and the associated p-value. Recognizing the potential exacerbation of the water-deficit condition

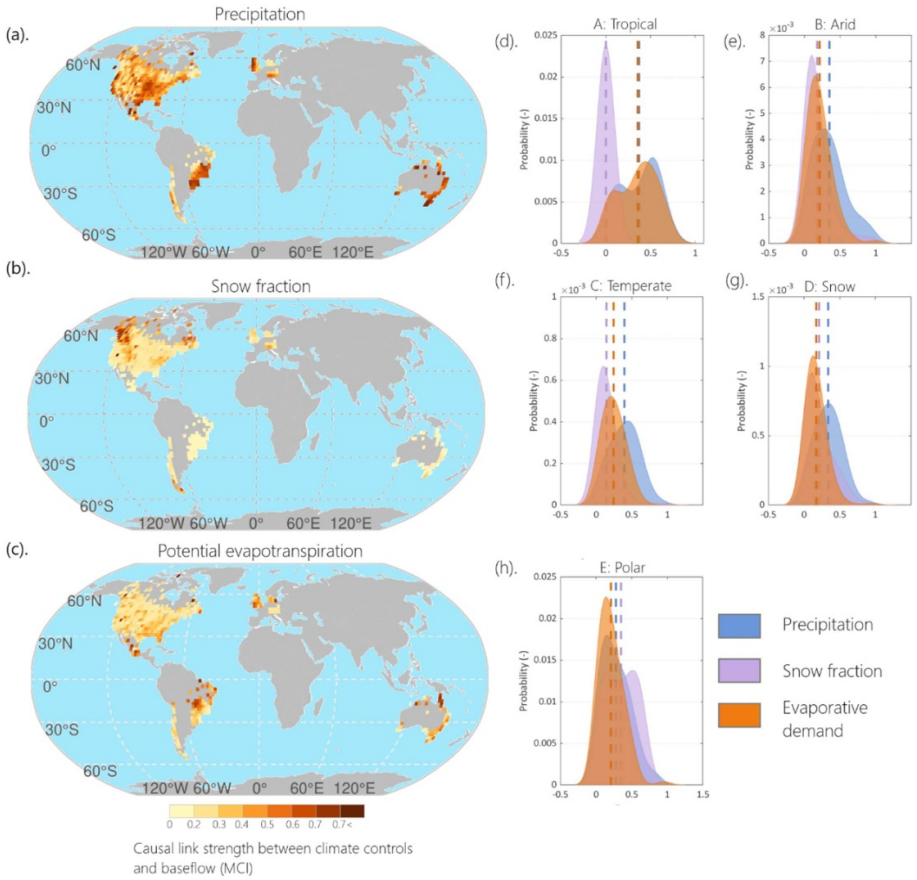

Figure 1. The absolute causal link strength between climate controls and baseflow. The strengths of causal links are measured in terms of MCI test statistic value, a normalized measure that quantifies the strength of causal relationships, with absolute MCI values ranging from 0 (weakest) to 1 (strongest). (a)–(c) display the spatial regional pattern of the averaged causal links between baseflow and climate controls—precipitation, snow fraction, and evaporative demand—represented in 25 by 25 km grids, respectively. This regional grid representation is for visualization purposes only, averaging observed station MCI values within each grid cell. (d)–(h) Show the kernel smoothed distribution of associated strength of causal links across the five major climate zones. The lines indicate the expected MCI values for each individual climate control.

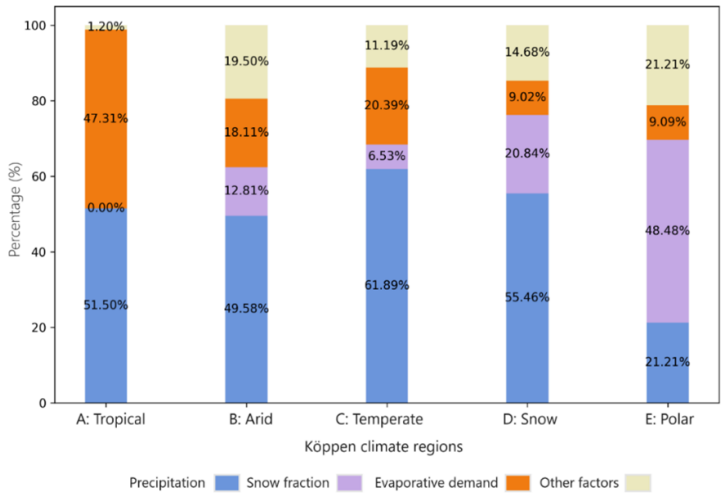

Figure 2. The relative occurrences of the three climatic factors (*i.e.* precipitation, evaporative demand, or snow fraction) as dominant controls of baseflow across five major climate regions as indicated by percentages. The climate regions depicted comprise the tropical climate zone (A), arid climate zone (B), temperate climate zone (C), cold climate zone (D), and polar climate zone (E). Each climatic driver's influence on baseflow is depicted in distinct colors, highlighting varying levels of influence across regions.

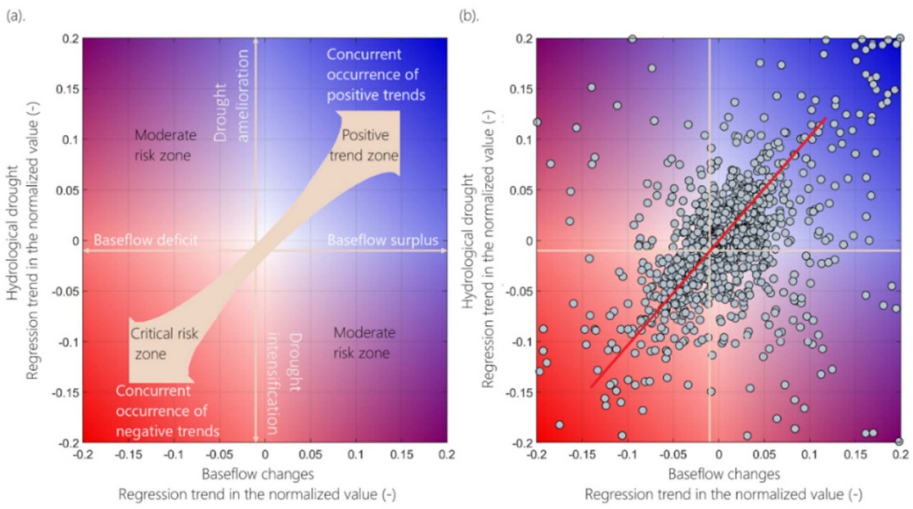

Figure 3. Global analysis of changes in normalized annual baseflows and hydrological drought. The ordinate represents the linear regression trend of normalized annual baseflow, while the abscissa depicts the linear regression trend of annual hydrologic droughts. In panel (a), the four zones are delineated by solid white lines, denoting the significance level (*i.e.* the associated trend magnitude) at p-value = 0.05. Concurrent conditions occur when both baseflow and hydrologic drought exhibit similar trend directions. The zone with negative trends for baseflow and hydrologic drought is called the critical risk zone, while the zones with either negative baseflow or negative hydrologic drought are termed moderate risk zones. The catchments with positive trends in both are placed in the positive trend zone. Panel (b) presents the results of the global analysis of 7168 Caravan catchments. The fitted linear regression line is shown in red in panel (b).

through groundwater extraction during hydrological droughts, we also examine the concurrent occurrence of baseflow changes and hydrological drought (figure 3). The abscissa represents the linear regression trend of normalized annual baseflow, while the ordinate illustrates the linear regression trend of normalized annual hydrological drought.

The four zones are delineated by two solid white lines indicating the significance threshold for a p-value of 0.05 (see figure 3(a)). This threshold is established to identify instances of physically unsustainable multi-year groundwater extraction coupled with hydrologic drought conditions—as defined by Margat *et al* [103] and Bierkens and Wada [104]. The critical risk zone exists where negative trends occur in both cases. The two zones in which either negative baseflow or hydrological drought happens are the moderate risk zones, while the one with both positive trends is the positive trend zone (figure 3(a)). Results are displayed in figure 3(b). The trend in baseflow demonstrates a strong association with hydrological droughts (Spearman $\rho = 0.59$). Of all catchments, 24% are in the critical risk zone and 31% are in the moderate risk zones. The remaining 45% are positioned in the positive trend zone, displaying a positive trend in both baseflow and hydrological droughts.

The preceding analysis revealed a significant correlation between baseflow and hydrologic droughts, given that they are both components of streamflow. Most trends are scattered around the fitted red line (figure 3(b)), with 69% of catchments falling within zones displaying similar directions in baseflow and hydrologic droughts. However, in some catchments, trends in hydrologic droughts deviate significantly from the fitted linear regression line, with 31% displaying opposing directions in their trends, which is partly associated to the changes in water inequality—defined as the unequal distribution of streamflow through a year, measured by the Gini index (see figure S4 in the supplementary information). In cases where baseflow increases but hydrological drought worsens, the Gini index rises, indicating increased streamflow inequality that exacerbates droughts. Conversely, when baseflow decreases but hydrological drought improves, the Gini index falls, signifying a more uniform streamflow distribution that mitigates drought severity.

We further investigated the spatial distribution of trends in normalized annual baseflow and annual hydrological drought (figure 4). Figures 4(a) and (b) reveal spatial patterns of regression trends in normalized baseflow and hydrologic drought, respectively. Figures 4(d) and (e) illustrate the corresponding probability distribution of trend magnitudes for baseflow and hydrologic drought.

In the northern hemisphere, negative trends in baseflows prevail in the northeastern part of Canada, the western US, and catchments near the Rockies. Conversely, positive trends in baseflow are mainly observed in the higher latitudes of Canada, including catchments in polar and snow climate regions. Hydrologic drought trends in the northern hemisphere align with baseflow trends but are often more intense, particularly in northern latitudes. In the southern hemisphere, catchments in Brazil with

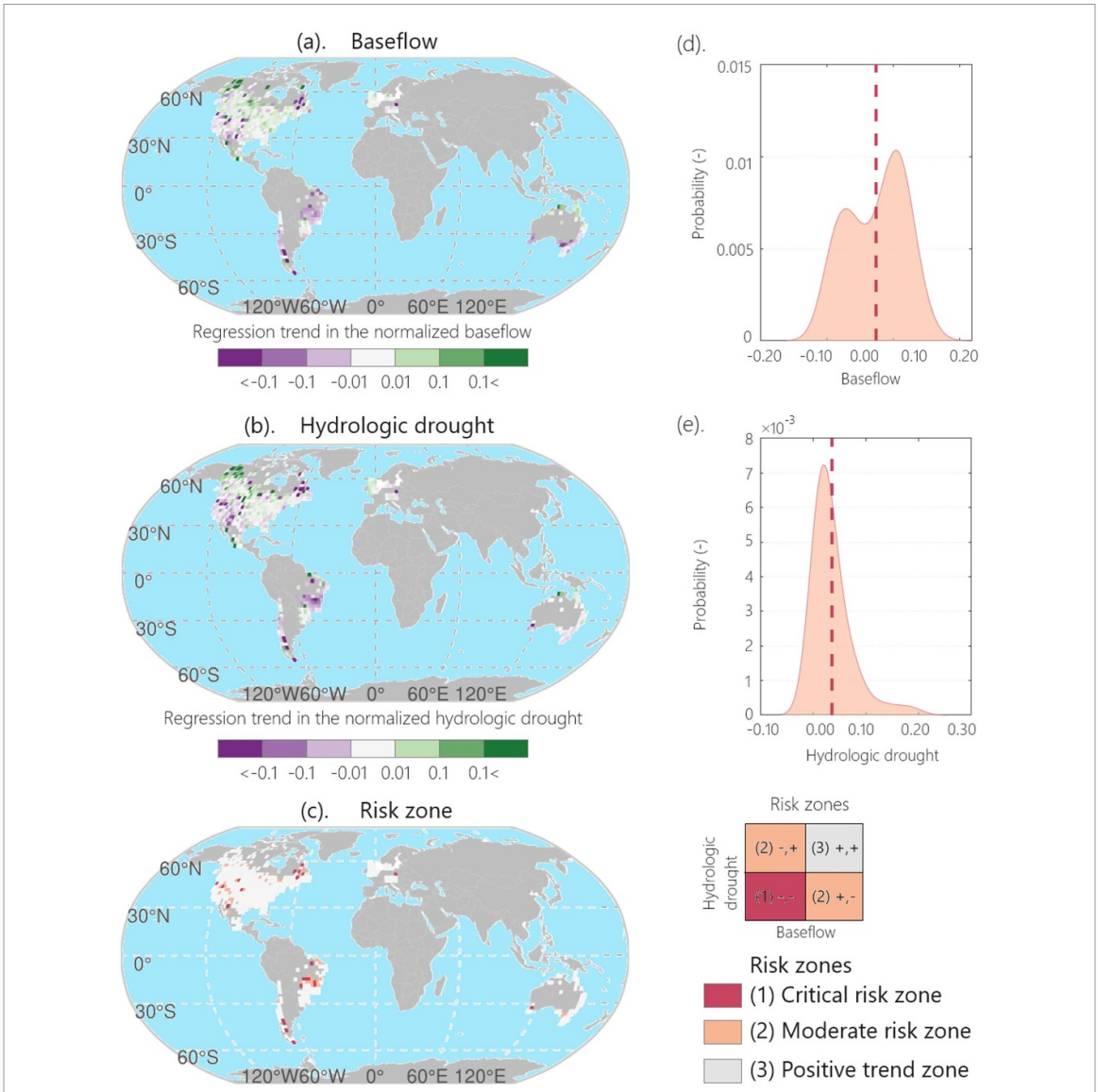

Figure 4. Spatial analysis of normalized baseflow and hydrologic drought changes in the Caravan catchments. (a) and (b) Illustrate the spatial distribution of regression trends in baseflow and hydrologic drought, respectively, with the significance level set at p-value = 0.05. The significant negative and positive trends are depicted in shades of purple and green, respectively. The corresponding probability distribution of trend values is shown in (d) and (e) for baseflow and hydrologic drought, respectively. (c) Highlights the spatial distribution of single or concurrent baseflow and hydrologic drought. Catchments with either negative baseflow or negative hydrologic drought are indicated in light red, representing a moderate risk. The catchments with the concurrent occurrence of negative baseflow and hydrologic drought are shown in dark red, designating critical risk zones; catchments with positive trends in baseflow and hydrologic drought are displayed in light grey, indicating a positive trend zone.

arid climates predominantly exhibit negative trends. Additionally, catchments along the Andes mountainous region with snow climates show negative trends. Some regions in southern Australia also display negative trends in baseflow. Hydrologic drought trends in the southern hemisphere generally align with baseflow trends, except for regions in southern Australia. The mean value of the regression trend across all catchments is 0.02 for baseflow and 0.03 for hydrologic droughts.

Figure 4(c) illustrates the spatial distribution of single or concurrent negative baseflow and hydrologic drought. Catchments with a moderate risk are indicated in light red, while those with critical risk conditions are shown in dark red; catchments belonging to the positive trend zone are displayed in light grey. In the northern hemisphere, catchments with a critical risk condition extend over the northeastern part of Canada, the western US, and some parts of the Rockies. Catchments with a moderate risk condition spread over some parts of northern Canada and most parts of the Rockies. In the southern hemisphere, catchments with a critical risk condition are situated in the central and northeast regions of Brazil and the Andes mountainous region, with some regions in the central

plateau of Brazil also exhibiting a moderate risk status.

4. Discussion

4.1. Limitations of the Budyko framework and the need for a novel approach

While traditional approaches like the Budyko framework have been used to analyze the sensitivity of baseflow to changes in climatic and physiographic controls, it has been shown that this framework originally designed for spatial, between-catchment analyses at long-term temporal scales, disregards substantial hydrological information [48]. To overcome these limitations and better understand the intricate interplay of climate factors and baseflow changes, we employ the PCMCI+ causal discovery algorithm. We used empirical data to focus on the causal effect of precipitation, snow fraction, and evaporative demand on baseflow changes and then analyzed the concurrent occurrence of trends in baseflow and hydrologic drought. Analyzing single/concurrent phenomena has implications for identifying key modulators, effective water resource management, climate impact assessment, and risk analyses.

4.2. Regional drivers of baseflow changes

Our findings showed that climate is an important modulator of the temporal changes in baseflow [1]. The global analysis of Caravan catchments identified precipitation as the primary driver of global baseflow changes with an average MCI of 0.45 across 58.3% of all catchments, aligning with findings of prior studies conducted across different catchments [9, 54, 105, 106]. For instance, in southwest China, research indicated that a negative trend in precipitation coupled with human activity, contributed to changes in baseflow [107]. Similarly, in China's Niya River basin, precipitation greatly impacted baseflow dynamics [108]. A large-scale analysis of natural catchments in the US, UK, Brazil, and Australia supports these findings, highlighting that precipitation exerts the most significant control on baseflow [109].

Evaporative demand emerged as the dominant control of baseflow in 17% of catchments, with an average MCI value of 0.30 across all studied catchments. This finding suggests that as climate warming intensifies, evaporative demand may deplete groundwater in catchments with shallow groundwater connections, as seen in previous studies [31, 110]. Our finding aligns with earlier research highlighting the association between baseflow changes in Costa Rica's tropical wet forest and groundwater withdrawal by the forest for evapotranspiration [33]. There are also studies that identified ET_p along with precipitation as primary controls, affecting baseflow changes at regional and global scales [37, 49, 80, 96, 109, 111]. Specifically, in the Loess Plateau, a semiarid climate region in China, research concluded that variations in baseflow are more sensitive to fluctuations in ET_p than in precipitation [45].

Snow fraction has emerged as the dominant control of baseflow changes, corroborating previous studies that highlight the significant role of the snow-to-precipitation ratio in governing summer flows in boreal headwater catchments [112]. This finding underscores the critical role snow fraction plays in sustaining baseflows, particularly in snow-dominated regions. However, with global warming, snow fraction is expected to decrease [77], which may lead to reduced snow accumulation and groundwater recharge, thereby diminishing baseflow during critical periods. This decline is likely to exacerbate low-flow conditions and negatively impact water availability in these catchments. In fact, snow fraction, among other climatic variables, is crucial in controlling runoff and low flows in the mountainous regions of western North America [113]. In southeastern Canada, temporal baseflow changes consistently align with snow fraction changes over the Oak Ridges Moraine [114]. Similarly, in the Midwestern US, it has been concluded that snow fraction stands out as the most influential factor in generating baseflow in fall and winter in the studied catchments [115].

4.3. Trends in baseflow and their implications

The analysis showed that negative trends in baseflow occur when either evaporative demand or snow fraction dominates precipitation in controlling baseflow changes. Specifically, we identify a negative trend in baseflow across the northern regions and the Rocky Mountains (catchments characterized by a cold climate), where the snow fraction emerges as the dominant control of baseflow changes. This observation aligns with previous findings, demonstrating the impact of changes in snow cover across much of Canada on alterations in baseflow dynamics [41]. In tropical catchments, however, a negative trend in the baseflow was observed where evaporative demand was identified as the primary control of baseflow changes. This confirmed earlier findings, demonstrating that ET_p affects groundwater under warming conditions, particularly in energy-limited systems [31]. However, it is important to note that the ERA5-Land datasets used in this study for estimating ET_p are based on the Penman–Monteith equation. While this method is commonly used in the literature [116–118], the choice of ET_p product could introduce variability in causal values (see figure S2 in the appendix). The physiological effect of increased atmospheric CO_2 on ET_p and drought conditions is also an important emerging topic. Elevated CO_2 levels can reduce the stomatal conductance of plants, potentially decreasing ET_p [119–123]. While this study did not explicitly account for CO_2 effects, future research should consider these physiological impacts to provide a more comprehensive understanding of baseflow changes under varying CO_2 scenarios.

4.4. Regional risk assessment and drought conditions

In the Northern Hemisphere, catchments exhibiting critical or moderate risk conditions were primarily located in eastern Canada, the western US, and the Rocky Mountains, while in the Southern Hemisphere, these catchments were concentrated on Brazil's central plateau and in the Andes mountain region. This concurs with prior findings, demonstrating that the western half of the US is experiencing drought conditions in the 21st century [124–129]. Studies also showed a decreasing trend in baseflow in the southwestern US, associated primarily with precipitation and to a lesser extent with evaporative demand and snowmelt [9, 67, 130]. Various local and regional studies align with our findings globally. The occurrence of hydrologic droughts and/or decreasing baseflow and their association with climatic factors have, for example, been documented in Canada [41, 131]. In eastern Canada, declining low flows have been linked to a reduction in snowfall [132]. In Brazil, the observed patterns of drought and baseflow and their association with climate factors align with prior findings, showing that decreasing precipitation and increasing water use occur in this region [95, 133]. In the Andes mountainous region, our findings of intensified drought and decreasing baseflow, driven by changes in precipitation and snow fraction aligned with the literature [134–137]. The concurrent condition of hydrologic drought and baseflow change, distinct from the individual occurrence of two phenomena is also investigated in this study. However, to some degree, the two phenomena are related [67]. Figure 4 indicates that catchments with intense hydrological droughts tend to be characterized by more prolonged baseflow loss than catchments with less pronounced changes. Catchments that experience the concurrent conditions often take much longer to recover from drought. This concurs with other studies in the literature that analyzed changes in terrestrial water storage and its relevance to drought severity using the GRACE satellite [12, 14, 138–142].

5. Conclusion

Our study demonstrates the significant role of climate factors—precipitation, snow fraction, and evaporative demand—in modulating baseflow changes across diverse regions. Using PCMCI+ causal discovery algorithm, we identified these key causal relationships that provide insights into the dynamics underlying baseflow variability. These findings underscore the importance of considering regional climatic drivers on baseflow dynamics, as certain factors become more prominent in specific climatic zones. For example, in tropical regions, evaporative demand may become a more critical factor, while in colder climates, snow fraction plays a critical role. Notably, the negative trends observed in baseflow in regions where snow fraction and evaporative demand are prominent controls, highlight the need for ongoing monitoring and adaptation strategies in water resource management.

Future research should aim to understand the complex interactions between climate, land surface processes, and human activities on baseflow dynamics. This includes investigating the effects of increased atmospheric CO2 and other emerging factors on baseflow and hydrological droughts. By continuing to refine our understanding of these complex interactions, we can better prepare for and mitigate the impacts of climate change on water resources.

Data availability statement

The data that support the findings of this study are openly available at the following URL/DOI: https://doi.org/10.5281/zenodo.7540792.

Acknowledgment

We gratefully acknowledge the financial support provided by the Natural Sciences and Engineering Research Council of Canada (NSERC Discovery Grant: RGPIN-2019-06894). We sincerely appreciate the detailed and constructive comments from the three anonymous reviewers, which have greatly enhanced this paper. A S B acknowledges São Paulo Research Foundation—FAPESP (2020/08140-0 and 2022/06017-1) for the scientific and financial support.

Data and code availability statement

Daily hydro-meteorological timeseries and catchment attributes are available from the Caravan dataset available at https://zenodo.org/records/7387919. The code to estimate the causal network can be obtained from Potsdam Institute for Climate Impact Research (PIK) available at https://tocsy.pik-potsdam.de/tigramite.php.

Conflict of interest

The authors declare no competing interests.

Appendix

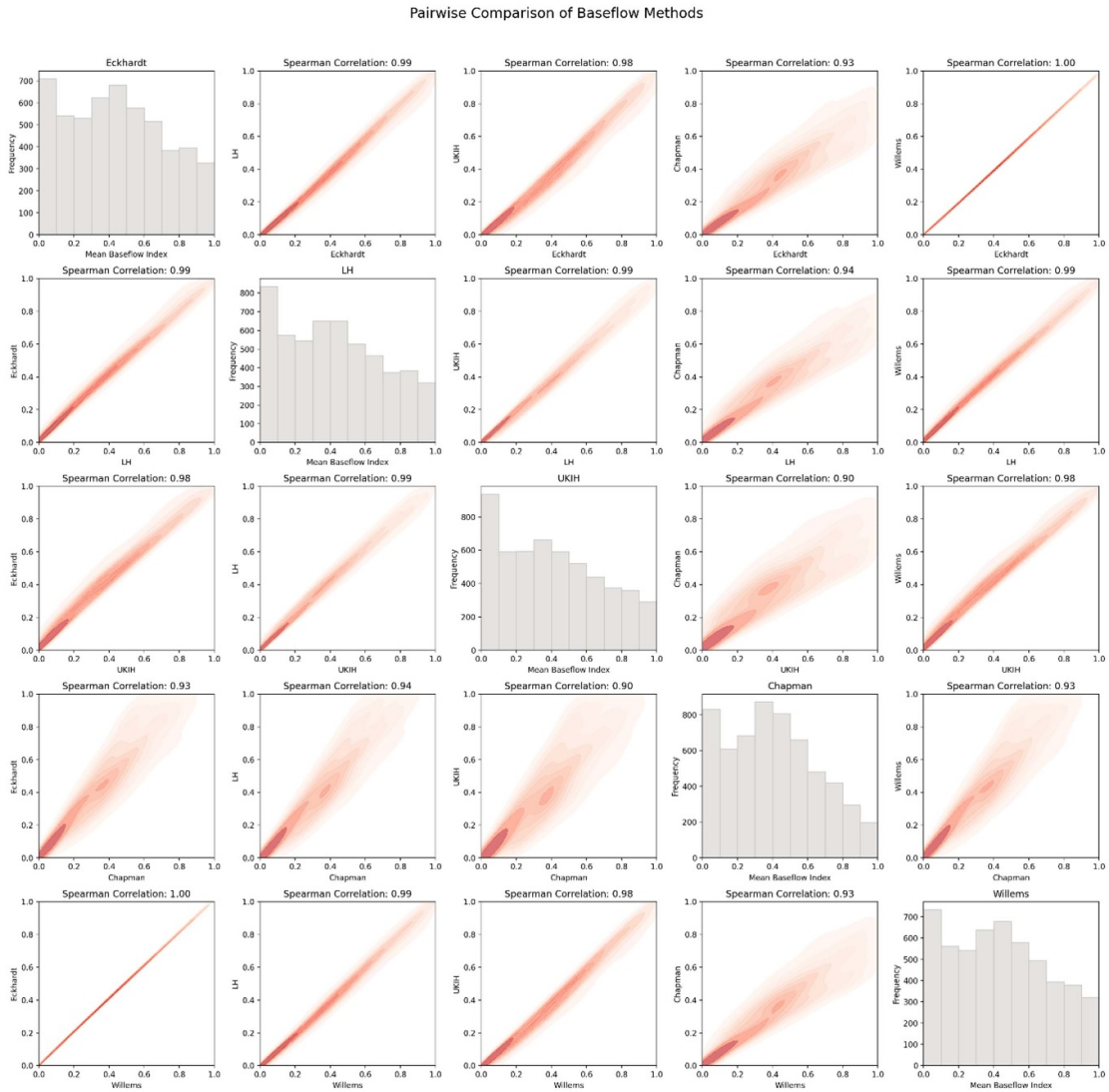

Figure S1. Pairwise comparison of five different streamflow partitioning methods: Lyne and Hollick filter pass (LH; Lyne and Hollick [81]), graphical method developed by UK Institute of Hydrology (UKIH; Aksoy *et al* [90]), Fixed interval graphical method from HYSEP program (Fixed; Sloto and Crouse [91]), Eckhardt filter (Eckhardt; Eckhardt [3]), and Chapman filter (Chapman; Chapman [92]). The values shown in each panel represent the Spearman correlation coefficients between the baseflow time series obtained from the different methods, ranging from 0.90 to 1.0, indicating the consistency across these methods.

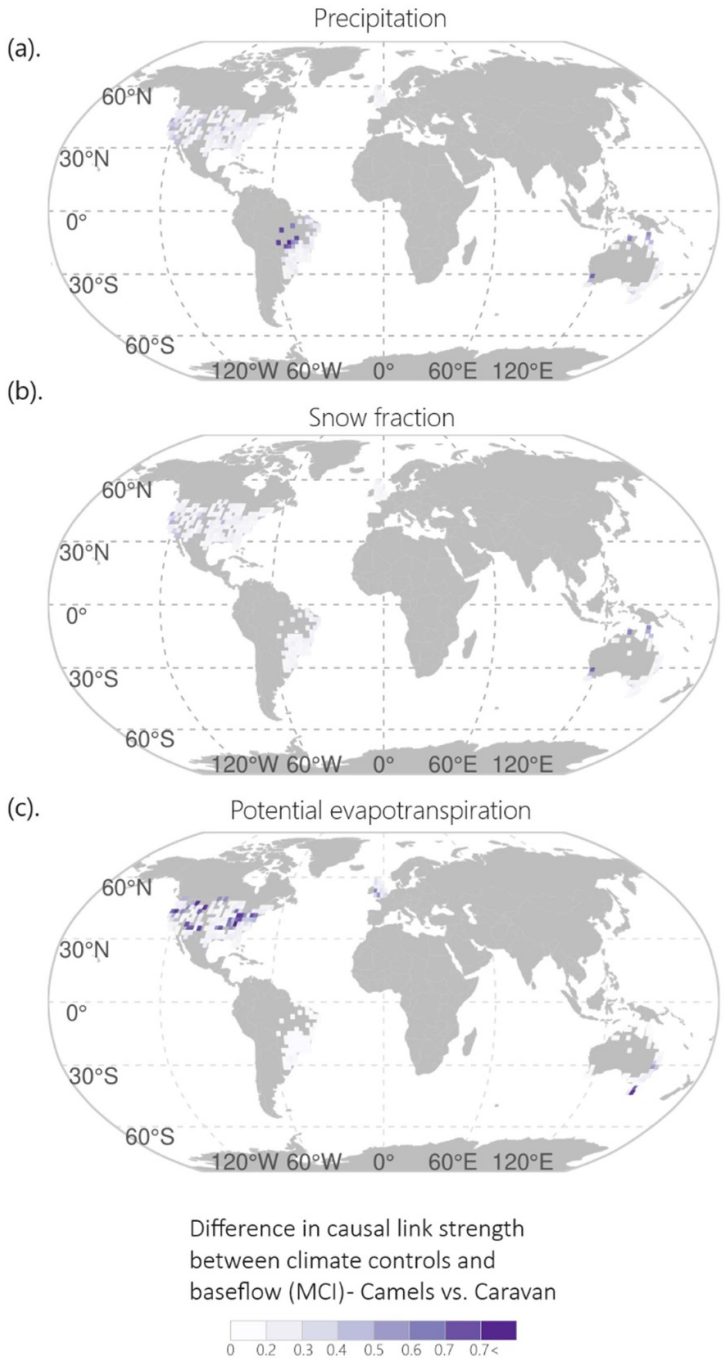

Figure S2. Difference in the absolute causal link strength between climate controls and baseflow (MCI) for four CAMELS (CAMELS-US, CAMELS-GB, CAMELS-AUS, and CAMELS-BR) versus Caravan datasets. The causal link strengths are quantified using the MCI test statistic, which ranges from 0 (weakest) to 1 (strongest). Panels (a)–(c) show the regional patterns of these differences across 25 × 25 km grids, illustrating variations in the absolute MCI values between the two datasets.

Spatial distribution of dominant controls of baseflow

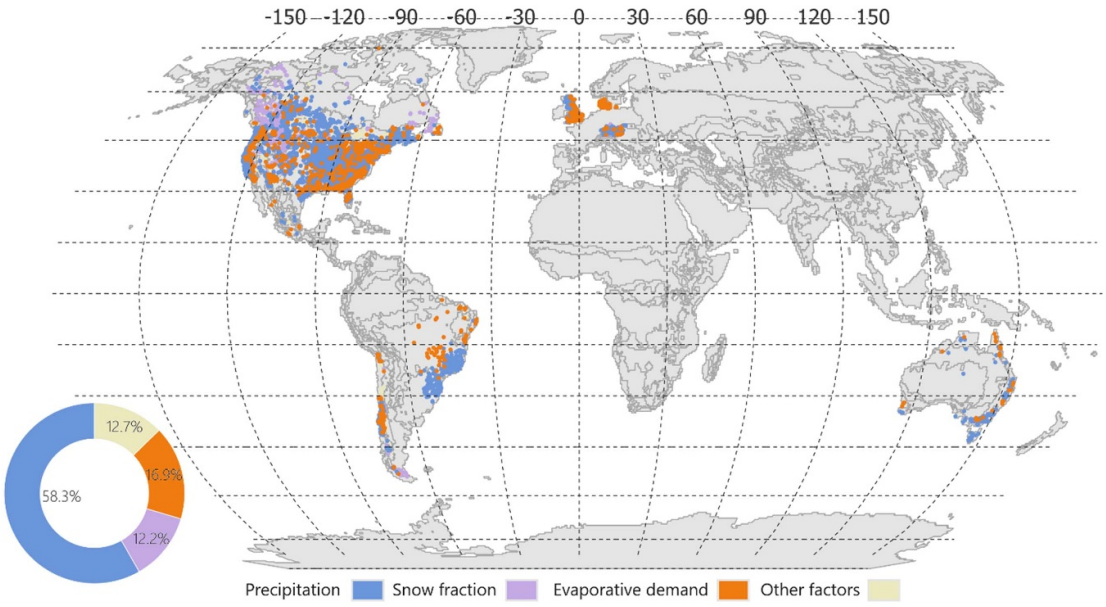

Figure S3. Spatial distribution of dominant controls influencing baseflow changes across 7138 catchments. The primary climate control, determined by the highest MCI value within each catchment, is designated as the dominant control. In cases where none of the three climate factors (precipitation, evaporative demand, or snow fraction) demonstrate a significant causal-effect relationship with baseflow, 'other factors' are considered the dominant control. The significance level is set at 0.05 level for independence tests. Colors denote the causative controls on baseflow changes. The donut chart shows the percentage of catchments in which each climate factor is dominant.

Analysis of Gini index and its relationship to the departures of trends in baseflow and hydrologic drought

To explain the opposing trend directions in the baseflow and hydrologic drought in figure 3, we employ the residuals of the fitted linear regression and the Gini index—a measure of water inequality—defined as the unequal distribution of streamflow through the year [143]. We used the Gini index of streamflow as a measure of global streamflow inequality over the studied period. Recently used in hydrology to investigate global inequality of precipitation and streamflow [143, 144], the Gini index provides insights on the spatiotemporal distribution of water resources.

Our investigation explored the impact of streamflow inequality, an essential factor influencing water availability inequality, on the departure of trends in baseflow and hydrologic drought severity.

The Gini index captures the annual inequality in streamflow at each gauge station, calculated by arranging daily streamflow values q in ascending order such that $q_i \leqslant q_{i+1}$ and can be expressed as [143]:

$$\text{Gini index} = \frac{1}{n}\left(n+1-2\left(\frac{\sum_{i=1}^{n}(n+1-i)\,q_i}{\sum_{i=1}^{n} q_i}\right)\right) \quad (2)$$

where n is the number of daily streamflow values available over each year. The Gini index ranges from 0 to 1, with 0 indicating a uniform distribution of streamflow throughout the year and 1 indicating that all flows transpire within a single day.

To explore temporal variations in streamflow inequality across the study period, we then calculated the trends in the annual Gini index. For each year, a singular Gini index was computed, and the linear regression trend in the yearly Gini index is analyzed to elucidate the temporal shifts in streamflow inequality for each gauge station. This analysis allowed us to unravel the evolving dynamics of global streamflow inequality over the examined timeframe and its relationship to the departure of trends in baseflow and hydrologic drought severity.

Our investigation aims to understand how temporal variations in streamflow inequality, denoted by the streamflow Gini, can account for these deviations (figure S2). The calculation involves determining the trend in the yearly streamflow Gini index, ranging from 0 to 1. A Gini index of 0 indicates a uniform flow distribution throughout the year, while a value of 1 indicates that all flows occur on a single day (Please see figure S5 for the results of expected Gini index across all catchments). The points of figure S4 are stratified with colors in panel (a). The residuals of the fitted linear regression line are then calculated, demonstrating the trend departures. The relationship between trends in the residuals and trends in the Gini index is depicted in panel (b) in figure S4.

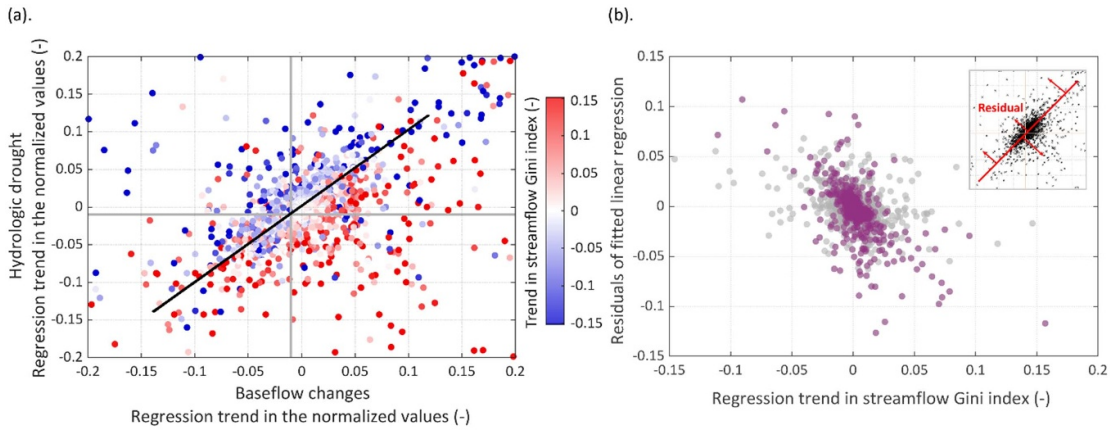

Figure S4. Analysis of departures of trends in the normalized annual baseflow and hydrologic drought. Panel (a) displays the trend in baseflow and hydrologic drought, stratified with trends in Gini index. Panel (b) explores the relationship between regression trend in streamflow Gini index and the residual of linear regression line fitted to points in panel (a), providing insights into the departure from the fitted line. In panel (b), the gray dots represent the residuals for all catchments, while the purple dots correspond to those within Zone 2.

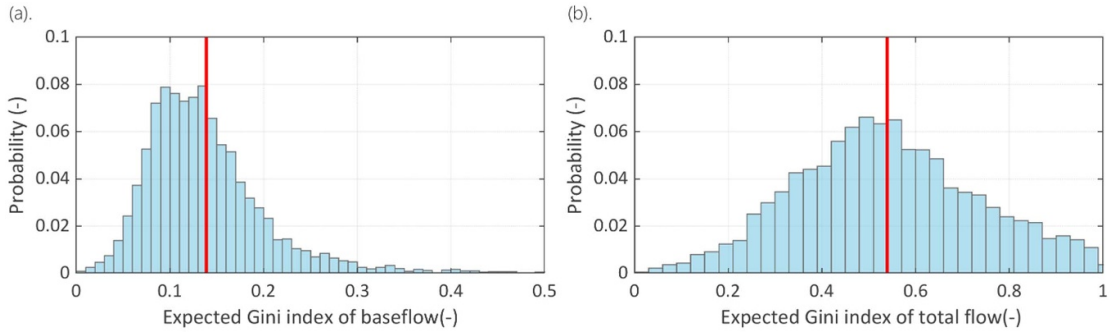

Figure S5. The analysis of Gini index for the 7138 catchments. Panels (a) and (b) display the distribution of expected Gini index for baseflow and total flow, respectively. The red lines are the expected value of the Gini index across all catchments.

Notably, the analysis reveals a significant association between changes in water inequality and the departure of trends from the fitted line across all catchments (depicted by light gray dots; Spearman $\rho = -0.51$). This association is even more pronounced for catchments situated in Zone 2, exhibiting a greater departure from the fitted line (depicted by purple dots; Spearman $\rho = -0.62$). Examining catchments below the fitted line reveals predominantly positive trends, indicating a shift towards less uniform streamflow distribution. Most catchments in this scenario are colored red, indicating that despite the rise in baseflow, drought conditions are worsening. This is likely due to a less uniform distribution of streamflow throughout the year, as evidenced by a higher Gini index. The increased inequality in streamflow exacerbates drought conditions by concentrating water flows into shorter, intense periods, leaving less water available during prolonged dry spells. Conversely, in the second case, baseflow decreases while hydrological drought flow improves. This improvement, despite lower baseflow, is driven by a more uniform distribution of streamflow, reflected in a lower Gini index. A more even water distribution across seasons helps mitigate the adverse effects of reduced baseflow, ensuring more consistent water availability and lessening the impact of drought.

ORCID iDs

Masoud Zaerpour https://orcid.org/0000-0002-5986-1628
Shadi Hatami https://orcid.org/0000-0002-0048-8144
André S Ballarin https://orcid.org/0000-0001-6997-8662
Simon Michael Papalexiou https://orcid.org/0000-0001-5633-0154
Alain Pietroniro https://orcid.org/0000-0001-5792-9177

References

[1] Tan X, Liu B and Tan X 2020 Global changes in baseflow under the impacts of changing climate and vegetation *Water Resour. Res.* **56** e2020WR027349

[2] Hayashi M and Rosenberry D O 2002 Effects of ground water exchange on the hydrology and ecology of surface water *Groundwater* **40** 309–16

[3] Eckhardt K 2005 How to construct recursive digital filters for baseflow separation *Hydrol. Process.* **19** 507–15

[4] Hellwig J and Stahl K 2018 An assessment of trends and potential future changes in groundwater-baseflow drought based on catchment response times *Hydrol. Earth Syst. Sci.* **22** 6209–24

[5] Hellwig J, Stoelzle M and Stahl K 2021 Groundwater and baseflow drought responses to synthetic recharge stress tests *Hydrol. Earth Syst. Sci.* **25** 1053–68

[6] Eltahir E A B and Yeh P J-F 1999 On the asymmetric response of aquifer water level to floods and droughts in Illinois *Water Resour. Res.* **35** 1199–217

[7] Peters E, Torfs P J J F, van Lanen H A J and Bier G 2003 Propagation of drought through groundwater—a new approach using linear reservoir theory *Hydrol. Process.* **17** 3023–40

[8] Castle S L, Thomas B F, Reager J T, Rodell M, Swenson S C and Famiglietti J S 2014 Groundwater depletion during drought threatens future water security of the Colorado River Basin *Geophys. Res. Lett.* **41** 5904–11

[9] Ficklin D L, Robeson S M and Knouft J H 2016 Impacts of recent climate change on trends in baseflow and stormflow in United States watersheds *Geophys. Res. Lett.* **43** 5079–88

[10] Ahiablame L, Sheshukov A Y, Rahmani V and Moriasi D 2017 Annual baseflow variations as influenced by climate variability and agricultural land use change in the Missouri River Basin *J. Hydrol.* **551** 188–202

[11] Miller M P, Buto S G, Susong D D and Rumsey C A 2016 The importance of base flow in sustaining surface water flow in the Upper Colorado River Basin *Water Resour. Res.* **52** 3547–62

[12] Pokhrel Y *et al* 2021 Global terrestrial water storage and drought severity under climate change *Nat. Clim. Change* **11** 226–33

[13] Li Q, Wei X, Zhang M, Liu W, Giles-Hansen K and Wang Y 2018 The cumulative effects of forest disturbance and climate variability on streamflow components in a large forest-dominated watershed *J. Hydrol.* **557** 448–59

[14] Houborg R, Rodell M, Li B, Reichle R and Zaitchik B F 2012 Drought indicators based on model-assimilated gravity recovery and climate experiment (GRACE) terrestrial water storage observations *Water Resour. Res.* **48** 7

[15] Gleeson T, Befus K M, Jasechko S, Luijendijk E and Cardenas M B 2016 The global volume and distribution of modern groundwater *Nat. Geosci.* **9** 161–7

[16] Wada Y, Wisser D and Bierkens M F P 2014 Global modeling of withdrawal, allocation and consumptive use of surface water and groundwater resources *Earth Syst. Dyn.* **5** 15–40

[17] Long D, Scanlon B R, Longuevergne L, Sun A Y, Fernando D N and Save H 2013 GRACE satellite monitoring of large depletion in water storage in response to the 2011 drought in Texas *Geophys. Res. Lett.* **40** 3395–401

[18] Ayers J R, Villarini G, Jones C and Schilling K 2019 Changes in monthly baseflow across the U.S *Midwest. Hydrol. Process.* **33** 748–58

[19] Zhao G, Kong L, Li Y, Xu Y and Li Z 2022 Investigating historical baseflow characteristics and variations in the Upper Yellow River Basin, China *Int. J. Environ. Res. Public Health* **19** 9267

[20] Ayers J R, Villarini G, Tramblay Y and Kim H 2023 Observed changes in monthly baseflow across Africa *Hydrol. Sci. J.* **68** 108–18

[21] Doble R, Walker G, Crosbie R, Guillaume J and Doody T 2023 An overview of groundwater response to a changing climate in the Murray-Darling Basin, Australia: potential implications for the basin system and opportunities for management *Hydrogeol. J.* **32** 59–80

[22] Peterson T J, Saft M, Peel M C and John A 2021 Watersheds may not recover from drought *Science* **372** 745–9

[23] Hughes J D, Petrone K C and Silberstein R P 2012 Drought, groundwater storage and stream flow decline in southwestern Australia *Geophys. Res. Lett.* **39** 3

[24] Saft M, Peel M C, Western A W and Zhang L 2016 Predicting shifts in rainfall-runoff partitioning during multiyear drought: roles of dry period and catchment characteristics *Water Resour. Res.* **52** 9290–305

[25] Ide T 2023 Climate change and Australia's national security *Aust. J. Int. Affairs* **77** 26–44

[26] Piniewski M, Eini M R, Chattopadhyay S, Okruszko T and Kundzewicz Z W 2022 Is there a coherence in observed and projected changes in riverine low flow indices across Central Europe? *Earth Sci. Rev.* **233** 104187

[27] Bloomfield J P, Marchant B P, Bricker S H and Morgan R B 2015 Regional analysis of groundwater droughts using hydrograph classification *Hydrol. Earth Syst. Sci.* **19** 4327–44

[28] Jasechko S, Seybold H, Perrone D, Fan Y and Kirchner J W 2021 Widespread potential loss of streamflow into underlying aquifers across the USA *Nature* **591** 391–5

[29] Jasechko S and Perrone D 2021 Global groundwater wells at risk of running dry *Science* **372** 418–21

[30] Miller O L, Miller M P, Longley P C, Alder J R, Bearup L A, Pruitt T, Jones D K, Putman A L, Rumsey C A and McKinney T 2021 How will baseflow respond to climate change in the upper colorado river basin? *Geophys. Res. Lett.* **48** e2021GL095085

[31] Condon L E, Atchley A L and Maxwell R M 2020 Evapotranspiration depletes groundwater under warming over the contiguous United States *Nat. Commun.* **11** 873

[32] Pavlovskii I, Jiang Y, Danielescu S and Kurylyk B L 2023 Influence of precipitation event magnitude on baseflow and coastal nitrate export for Prince Edward Island, Canada *Hydrol. Process.* **37** e14892

[33] Cadol D, Kampf S and Wohl E 2012 Effects of evapotranspiration on baseflow in a tropical headwater catchment *J. Hydrol.* **462–463** 4–14

[34] Jenicek M and Ledvinka O 2020 Importance of snowmelt contribution to seasonal runoff and summer low flows in Czechia *Hydrol. Earth Syst. Sci.* **24** 3475–91

[35] Le E, Janssen J, Hammond J and Ameli A A 2023 The persistence of snow on the ground affects the shape of streamflow hydrographs over space and time: a continental-scale analysis *Front. Environ. Sci.* **11** 1207508

[36] Milly P C D and Dunne K A 2020 Colorado River flow dwindles as warming-driven loss of reflective snow energizes evaporation *Science* **367** 1252–5

[37] Yao L, Sankarasubramanian A and Wang D 2021 Climatic and landscape controls on long-term baseflow *Water Resour. Res.* **57** e2020WR029284

[38] Meira Neto A A, Niu G-Y, Roy T, Tyler S and Troch P A 2020 Interactions between snow cover and evaporation lead to higher sensitivity of streamflow to temperature *Commun. Earth Environ.* **1** 1–7

[39] Jenicek M, Hnilica J, Nedelcev O and Sipek V 2021 Future changes in snowpack will impact seasonal runoff and low flows in Czechia *J. Hydrol.* **37** 100899

[40] Li H, Wang W, Fu J, Chen Z, Ning Z and Liu Y 2021 Quantifying the relative contribution of climate variability and human activities impacts on baseflow dynamics in the Tarim River Basin, Northwest China *J. Hydrol.* **36** 100853

[41] Murray J, Ayers J and Brookfield A 2023 The impact of climate change on monthly baseflow trends across Canada *J. Hydrol.* **618** 129254

[42] Berghuijs W R, Larsen J R, van Emmerik T H M and Woods R A 2017 A global assessment of runoff sensitivity to changes in precipitation, potential evaporation, and other factors *Water Resour. Res.* **53** 8475–86
[43] Cheng S, Cheng L, Liu P, Qin S, Zhang L, Xu C-Y, Xiong L, Liu L and Xia J 2021 An analytical baseflow coefficient curve for depicting the spatial variability of mean annual catchment baseflow *Water Resour. Res.* **57** e2020WR029529
[44] Gnann S J, Woods R A and Howden N J K 2019 Is there a baseflow budyko curve? *Water Resour. Res.* **55** 2838–55
[45] Wu J, Miao C, Duan Q, Lei X, Li X and Li H 2019 Dynamics and attributions of baseflow in the semiarid loess plateau *J. Geophys. Res.: Atmos.* **124** 3684–701
[46] Zaerpour M, Hatami S, Sadri J and Nazemi A 2021 A global algorithm for identifying changing streamflow regimes: application to Canadian natural streams (1966–2010) *Hydrol. Earth Syst. Sci.* **25** 5193–217
[47] Zaerpour M, Papalexiou S M and Nazemi A 2021 Informing stochastic streamflow generation by large-scale climate indices at single and multiple sites *Adv. Water Resour.* **156** 104037
[48] Berghuijs W R and Woods R A 2016 Correspondence: space-time asymmetry undermines water yield assessment *Nat. Commun.* **7** 11603
[49] Meira Neto A A, Roy T, de Oliveira P T S and Troch P A 2020 An aridity index-based formulation of streamflow components *Water Resour. Res.* **56** e2020WR027123
[50] Ballarin A S, Oliveira P T S, Marchezepe B K, Godoi R F, Campos A M, Campos F S, Almagro A and Meira Neto A A 2022 The impact of an open water balance assumption on understanding the factors controlling the long-term streamflow components *Water Resour. Res.* **58** e2022WR032413
[51] Bloomfield J P, Allen D J and Griffiths K J 2009 Examining geological controls on baseflow index (BFI) using regression analysis: an illustration from the Thames Basin, UK *J. Hydrol.* **373** 164–76
[52] Brandes D, Hoffmann J G and Mangarillo J T 2005 Base flow recession rates, low flows, and hydrologic features of small watersheds in Pennsylvania, USA[1] *JAWRA J. Am. Water Resour. Assoc.* **41** 1177–86
[53] Longobardi A and Villani P 2008 Baseflow index regionalization analysis in a mediterranean area and data scarcity context: role of the catchment permeability index *J. Hydrol.* **355** 63–75
[54] Rumsey C A, Miller M P, Susong D D, Tillman F D and Anning D W 2015 Regional scale estimates of baseflow and factors influencing baseflow in the Upper Colorado River Basin *J. Hydrol.* **4** 91–107
[55] Cheng L, Zhang L, Chiew F H S, Canadell J G, Zhao F, Wang Y-P, Hu X and Lin K 2017 Quantifying the impacts of vegetation changes on catchment storage-discharge dynamics using paired-catchment data *Water Resour. Res.* **53** 5963–79
[56] Karlsen R H, Grabs T, Bishop K, Buffam I, Laudon H and Seibert J 2016 Landscape controls on spatiotemporal discharge variability in a boreal catchment *Water Resour. Res.* **52** 6541–56
[57] Runge J *et al* 2019 Inferring causation from time series in Earth system sciences *Nat. Commun.* **10** 2553
[58] Runge J, Nowack P, Kretschmer M, Flaxman S and Sejdinovic D 2019 Detecting and quantifying causal associations in large nonlinear time series datasets *Sci. Adv.* **5** eaau4996
[59] Runge J 2020 Discovering contemporaneous and lagged causal relations in autocorrelated nonlinear time series datasets *Proc. 36th Conf. on Uncertainty in Artificial Intelligence (UAI)* (PMLR) pp 1388–97
[60] Runge J, Petoukhov V, Donges J F, Hlinka J, Jajcay N, Vejmelka M, Hartman D, Marwan N, Paluš M and Kurths J 2015 Identifying causal gateways and mediators in complex spatio-temporal systems *Nat. Commun.* **6** 8502
[61] Nowack P, Runge J, Eyring V and Haigh J D 2020 Causal networks for climate model evaluation and constrained projections *Nat. Commun.* **11** 1415
[62] Runge J 2018 Causal network reconstruction from time series: from theoretical assumptions to practical estimation *Chaos Interdiscip. J. Nonlinear Sci.* **28** 075310
[63] Delforge D, de Viron O, Vanclooster M, Van Camp M and Watlet A 2022 Detecting hydrological connectivity using causal inference from time series: synthetic and real karstic case studies *Hydrol. Earth Syst. Sci.* **26** 2181–99
[64] Almendra-Martín L, Martínez-Fernández J, Piles M, González-Zamora Á, Benito-Verdugo P and Gaona J 2022 Influence of atmospheric patterns on soil moisture dynamics in Europe *Sci. Total Environ.* **846** 157537
[65] He X, Wada Y, Wanders N and Sheffield J 2017 Intensification of hydrological drought in California by human water management *Geophys. Res. Lett.* **44** 1777–85
[66] Gu L, Yin J, Slater L J, Chen J, Do H X, Wang H-M, Chen L, Jiang Z and Zhao T 2023 Intensification of global hydrological droughts under anthropogenic climate warming *Water Resour. Res.* **59** e2022WR032997
[67] Johnson K, Harpold A, Carroll R W H, Barnard H, Raleigh M S, Segura C, Li L, Williams K H, Dong W and Sullivan P L 2023 Leveraging groundwater dynamics to improve predictions of summer low-flow discharges *Water Resour. Res.* **59** e2023WR035126
[68] Kratzert F *et al* 2023 Caravan—A global community dataset for large-sample hydrology *Sci. Data* **10** 61
[69] Fowler K J A, Acharya S C, Addor N, Chou C and Peel M C 2021 CAMELS-AUS: hydrometeorological time series and landscape attributes for 222 catchments in Australia *Earth Syst. Sci. Data* **13** 3847–67
[70] Chagas V B P, Chaffe P L B, Addor N, Fan F M, Fleischmann A S, Paiva R C D and Siqueira V A 2020 CAMELS-BR: hydrometeorological time series and landscape attributes for 897 catchments in Brazil *Earth Syst. Sci. Data* **12** 2075–96
[71] Alvarez-Garreton C *et al* 2018 The CAMELS-CL dataset: catchment attributes and meteorology for large sample studies—Chile dataset *Hydrol. Earth Syst. Sci.* **22** 5817–46
[72] Coxon G *et al* 2020 CAMELS-GB: hydrometeorological time series and landscape attributes for 671 catchments in Great Britain *Earth Syst. Sci. Data* **12** 2459–83
[73] Addor N, Newman A J, Mizukami N and Clark M P 2017 The CAMELS data set: catchment attributes and meteorology for large-sample studies *Hydrol. Earth Syst. Sci.* **21** 5293–313
[74] Hersbach H *et al* 2020 The ERA5 global reanalysis *Q. J. R. Meteorol. Soc.* **146** 1999–2049
[75] Pipatsitee P, Ninsawat S, Tripathi N K, Shanmugam M and Chitsutti P 2023 Estimating daily potential evapotranspiration using GNSS-based precipitable water vapor *Heliyon* **9** e17747
[76] Xu C, Wang W, Hu Y and Liu Y 2024 Evaluation of ERA5, ERA5-Land, GLDAS-2.1, and GLEAM potential evapotranspiration data over mainland China *J. Hydrol.* **51** 101651
[77] Berghuijs W R, Woods R A and Hrachowitz M 2014 A precipitation shift from snow towards rain leads to a decrease in streamflow *Nat. Clim. Change* **4** 583–6
[78] Hock R 2003 Temperature index melt modelling in mountain areas *J. Hydrol.* **282** 104–15
[79] Knoben W J M, Woods R A and Freer J E 2018 A quantitative hydrological climate classification evaluated with independent streamflow data *Water Resour. Res.* **54** 5088–109
[80] Sivapalan M, Yaeger M A, Harman C J, Xu X and Troch P A 2011 Functional model of water balance variability at the catchment scale: 1. Evidence of hydrologic similarity and space-time symmetry *Water Resour. Res.* **47** 2

[81] Lyne V and Hollick M 1979 Stochastic time variable rainfall-runoff modelling (available at: https://scholar.google.com/scholar_lookup?hl=en&publication_year=1979&pages=82-92&author=V.+D.+Lyne&author=M.+Hollick&title=Hydrology+and+water+resources+symposium)
[82] Trancoso R, Larsen J R, McVicar T R, Phinn S R and McAlpine C A 2017 CO2-vegetation feedbacks and other climate changes implicated in reducing base flow *Geophys. Res. Lett.* **44** 2310–8
[83] Arnold J G and Allen P M 1999 Automated methods for estimating baseflow and ground water recharge from streamflow records[1] *JAWRA J. Am. Water Resour. Assoc.* **35** 411–24
[84] Nathan R J and McMahon T A 1990 Evaluation of automated techniques for base flow and recession analyses *Water Resour. Res.* **26** 1465–73
[85] Lee S and Ajami H 2023 Comprehensive assessment of baseflow responses to long-term meteorological droughts across the United States *J. Hydrol.* **626** 130256
[86] Gnann S J, McMillan H K, Woods R A and Howden N J K 2021 Including regional knowledge improves baseflow signature predictions in large sample hydrology *Water Resour. Res.* **57** e2020WR028354
[87] Berghuijs W R and Slater L J 2023 Groundwater shapes North American river floods *Environ. Res. Lett.* **18** 034043
[88] Ladson A R, Brown R, Neal B and Nathan R 2013 A standard approach to baseflow separation using the Lyne and Hollick filter *Australas. J. Water Resour.* **17** 25–34
[89] Zhang J, Zhang Y, Song J and Cheng L 2017 Evaluating relative merits of four baseflow separation methods in Eastern Australia *J. Hydrol.* **549** 252–63
[90] Aksoy H, Kurt I and Eris E 2009 Filtered smoothed minima baseflow separation method *J. Hydrol.* **372** 94–101
[91] Sloto R A and Crouse M Y 1996 HYSEP: a computer program for streamflow hydrograph separation and analysis *Water-Resources Investigations Report* (available at: https://pubs.usgs.gov/publication/wri964040)
[92] Chapman T G 1991 Comment on "Evaluation of automated techniques for base flow and recession analyses" by R. J. Nathan and T. A. McMahon *Water Resour. Res.* **27** 1783–4
[93] Stahl K, Hisdal H, Hannaford J, Tallaksen L M, van Lanen H A J, Sauquet E, Demuth S, Fendekova M and Jódar J 2010 Streamflow trends in Europe: evidence from a dataset of near-natural catchments *Hydrol. Earth Syst. Sci.* **14** 2367–82
[94] Wilhite D and Buchanan-Smith M 2005 Drought as hazard: understanding the natural and social context *Drought and Water Crisis: Science, Technology, and Management Issues* vol 3–28 (Taylor and Francis)
[95] Chagas V B P, Chaffe P L B and Blöschl G 2022 Climate and land management accelerate the Brazilian water cycle *Nat. Commun.* **13** 5136
[96] Beck H E, van Dijk A I, Miralles D G, de Jeu R A M, (Sampurno) Bruijnzeel L A, McVicar T R and Schellekens J 2013 Global patterns in base flow index and recession based on streamflow observations from 3394 catchments *Water Resour. Res.* **49** 7843–63
[97] Peña-Arancibia J L, van Dijk A I, Mulligan M and Bruijnzeel L A 2010 The role of climatic and terrain attributes in estimating baseflow recession in tropical catchments *Hydrol. Earth Syst. Sci.* **14** 2193–205
[98] Van Dijk A I 2010 Climate and terrain factors explaining streamflow response and recession in Australian catchments *Hydrol. Earth Syst. Sci.* **14** 159–69
[99] Galytska E, Weigel K, Handorf D, Jaiser R, Köhler R, Runge J and Eyring V 2023 Evaluating causal arctic-midlatitude teleconnections in CMIP6 *J. Geophys. Res.: Atmos.* **128** e2022JD037978
[100] Spirtes P, Glymour C N, Scheines R and Heckerman D 2000 *Causation, Prediction, and Search* (MIT Press)
[101] Runge J 2015 Quantifying information transfer and mediation along causal pathways in complex systems *Phys. Rev.* E **92** 062829
[102] Ombadi M, Nguyen P, Sorooshian S and Hsu K 2020 Evaluation of methods for causal discovery in hydrometeorological systems *Water Resour. Res.* **56** e2020WR027251
[103] Margat J, Foster S and Droubi A 2006 Concept and importance of non-renewable resources *Non-Renewable Groundwater Resources: A Guidebook on Socially-Sustainable Management for Water-Policy Makers* vol 10 (United Nations Educational, Scientific and Cultural Organization) pp 13–24
[104] Bierkens M F P and Wada Y 2019 Non-renewable groundwater use and groundwater depletion: a review *Environ. Res. Lett.* **14** 063002
[105] Zomlot Z, Verbeiren B, Huysmans M and Batelaan O 2015 Spatial distribution of groundwater recharge and base flow: assessment of controlling factors *J. Hydrol.* **4** 349–68
[106] Kundzewicz Z W and Döll P 2009 Will groundwater ease freshwater stress under climate change? *Hydrol. Sci. J.* **54** 665–75
[107] Mo C, Ruan Y, Xiao X, Lan H and Jin J 2021 Impact of climate change and human activities on the baseflow in a typical karst basin, Southwest China *Ecol. Indicators* **126** 107628
[108] Hu K, He J, Danierhan S and Tuerxun Y 2023 Sensitivity of river ecological baseflow to climate change in arid areas *Front. Environ. Sci.* **10** 1080810
[109] Chen S and Ruan X 2023 A hybrid Budyko-type regression framework for estimating baseflow from climate and catchment attributes *J. Hydrol.* **618** 129118
[110] Condon L E and Maxwell R M 2019 Simulating the sensitivity of evapotranspiration and streamflow to large-scale groundwater depletion *Sci. Adv.* **5** eaav4574
[111] Wang D and Wu L 2013 Similarity of climate control on base flow and perennial stream density in the Budyko framework *Hydrol. Earth Syst. Sci.* **17** 315–24
[112] Meriö L-J, Ala-aho P, Linjama J, Hjort J, Kløve B and Marttila H 2019 Snow to precipitation ratio controls catchment storage and summer flows in boreal headwater catchments *Water Resour. Res.* **55** 4096–109
[113] Dierauer J R, Whitfield P H and Allen D M 2018 Climate controls on runoff and low flows in mountain catchments of Western North America *Water Resour. Res.* **54** 7495–510
[114] Buttle J M, Greenwood W J and Gerber R E 2015 Spatiotemporal patterns of baseflow metrics for basins draining the Oak Ridges Moraine, southern Ontario, Canada *Can. Water Resour. J./Rev. Can. Ressour. Hydriques* **40** 3–22
[115] Huang S, Dong Q, Zhang X and Deng W 2021 Catchment natural driving factors and prediction of baseflow index for continental united states based on random forest technique *Stoch. Environ. Res. Risk Assess.* **35** 2567–81
[116] Muñoz-Sabater J *et al* 2021 ERA5-land: a state-of-the-art global reanalysis dataset for land applications *Earth Syst. Sci. Data* **13** 4349–83
[117] Xie W, Yi S, Leng C, Xia D, Li M, Zhong Z and Ye J 2022 The evaluation of IMERG and ERA5-land daily precipitation over China with considering the influence of gauge data bias *Sci. Rep.* **12** 8085
[118] Zhao P and He Z 2022 A first evaluation of ERA5-land reanalysis temperature product over the chinese qilian mountains *Front. Earth Sci.* **10** 907730
[119] Li F, Kang S and Zhang J 2004 Interactive effects of elevated CO_2, nitrogen and drought on leaf area, stomatal conductance, and evapotranspiration of wheat *Agric. Water Manage.* **67** 221–33
[120] Varghese F C and Mitra S 2024 Investigating the role of driving variables on ETo variability and

"evapotranspiration paradox" across the indian subcontinent under historic and future climate change *Water Resour. Manage.* **38** 5723–37
[121] Yeh S-W, Song S-Y, Allan R P, An S-I and Shin J 2021 Contrasting response of hydrological cycle over land and ocean to a changing CO_2 pathway *npj Clim. Atmos. Sci.* **4** 1–8
[122] Ballarin A S, Sousa Mota Uchôa J G, Dos Santos M S, Almagro A, Miranda I P, da Silva P G C, da Silva G J, Gomes Júnior M N, Wendland E and Oliveira P T S 2023 Brazilian water security threatened by climate change and human behavior *Water Resour. Res.* **59** e2023WR034914
[123] Yang Y, Roderick M L, Zhang S, McVicar T R and Donohue R J 2019 Hydrologic implications of vegetation response to elevated CO_2 in climate projections *Nat. Clim. Change* **9** 44–48
[124] Leeper R D, Bilotta R, Petersen B, Stiles C J, Heim R, Fuchs B, Prat O P, Palecki M and Ansari S 2022 Characterizing U.S. drought over the past 20 years using the U.S. drought monitor *Int. J. Climatol.* **42** 6616–30
[125] Cayan D R, Das T, Pierce D W, Barnett T P, Tyree M and Gershunov A 2010 Future dryness in the southwest US and the hydrology of the early 21st century drought *Proc. Natl Acad. Sci.* **107** 21271–6
[126] Buotte P C, Levis S, Law B E, Hudiburg T W, Rupp D E and Kent J J 2019 Near-future forest vulnerability to drought and fire varies across the western United States *Glob. Change Biol.* **25** 290–303
[127] Affram G, Zhang W, Hipps L and Ratterman C 2023 Characterizing the development and drivers of 2021 Western US drought *Environ. Res. Lett.* **18** 044040
[128] Brunner M I, Swain D L, Gilleland E and Wood A W 2021 Increasing importance of temperature as a contributor to the spatial extent of streamflow drought *Environ. Res. Lett.* **16** 024038
[129] Ficklin D L, Abatzoglou J T, Robeson S M, Null S E and Knouft J H 2018 Natural and managed watersheds show similar responses to recent climate change *Proc. Natl Acad. Sci.* **115** 8553–7
[130] Apurv T and Cai X 2020 Drought propagation in contiguous U.S. watersheds: a process-based understanding of the role of climate and watershed properties *Water Resour. Res.* **56** e2020WR027755
[131] Aygün O, Kinnard C and Campeau S 2020 Impacts of climate change on the hydrology of northern midlatitude cold regions *Prog. Phys. Geogr.: Earth Environ.* **44** 338–75
[132] Assani A, Zeroual A, Kinnard C and Roy A 2022 Spatial–temporal variability of seasonal daily minimum flows in southern Quebec: synthesis on the impacts of climate, agriculture and wetlands *Hydrol. Res.* **53** 1494–509
[133] Domingues L M and da Rocha H R 2022 Serial droughts and loss of hydrologic resilience in a subtropical basin: the case of water inflow into the Cantareira reservoir system in Brazil during 2013–2021 *J. Hydrol.* **44** 101235
[134] Drenkhan F, Huggel C, Hoyos N and Scott C A 2023 Hydrology, water resources availability and management in the Andes under climate change and human impacts *J. Hydrol.* **49** 101519
[135] Central and South America 2023 Climate change 2022—impacts, adaptation and vulnerability: working group II contribution to the sixth assessment report of the intergovernmental panel on climate change *Intergovernmental Panel on Climate Change (IPCC)* (Cambridge University Press) pp 1689–816
[136] Yáñez San Francisco E, Pascual Aguilar J A and MacDonell S 2023 Hydrological response of a headwater catchment in the semi-arid Andes (30°S) to climate change *J. Water Clim. Change* **14** 3617–34
[137] Vega-Briones J, de Jong S, Galleguillos M and Wanders N 2023 Identifying driving processes of drought recovery in the southern Andes natural catchments *J. Hydrol.* **47** 101369
[138] Zhao M, A G, Velicogna I and Kimball J S 2017 Satellite observations of regional drought severity in the continental united states using GRACE-based terrestrial water storage changes *J. Clim.* **30** 6297–308
[139] Rodell M, Famiglietti J S, Wiese D N, Reager J T, Beaudoing H K, Landerer F W and Lo M-H 2018 Emerging trends in global freshwater availability *Nature* **557** 651–9
[140] Thomas B F, Famiglietti J S, Landerer F W, Wiese D N, Molotch N P and Argus D F 2017 GRACE groundwater drought index: evaluation of california central valley groundwater drought *Remote Sens. Environ.* **198** 384–92
[141] Thomas A C, Reager J T, Famiglietti J S and Rodell M 2014 A GRACE-based water storage deficit approach for hydrological drought characterization *Geophys. Res. Lett.* **41** 1537–45
[142] Famiglietti J S, Lo M, Ho S L, Bethune J, Anderson K J, Syed T H, Swenson S C, de Linage C R and Rodell M 2011 Satellites measure recent rates of groundwater depletion in California's Central Valley *Geophys. Res. Lett.* **38** H11B–1169
[143] Kuntla S K, Saharia M, Prakash S and Villarini G 2024 Precipitation inequality exacerbates streamflow inequality, but dams moderate it *Sci. Total Environ.* **912** 169098
[144] Masaki Y, Hanasaki N, Takahashi K and Hijioka Y 2014 Global-scale analysis on future changes in flow regimes using Gini and Lorenz asymmetry coefficients *Water Resour. Res.* **50** 4054–78